Nuclear spin effects in biological processes

Ofek Vardi[a] (ID), Naama Maroudas-Sklare[a,b] (ID), Yuval Kolodny[a], Artem Volosniev[c] (ID), Amijai Saragovi[d], Nir Galili[e] (ID), Stav Ferrera[a], Areg Ghazaryan[c], Nir Yuran[a] (ID), Hagit P. Affek[f] (ID), Boaz Luz[f] (ID), Yonaton Goldsmith[f] (ID), Nir Keren[b] (ID), Shira Yochelis[a] (ID), Itay Halevy[e] (ID), Mikhail Lemeshko[c], and Yossi Paltiel[a,1]

Traditionally, nuclear spin is not considered to affect biological processes. Recently, this has changed as isotopic fractionation that deviates from classical mass dependence was reported both in vitro and in vivo. In these cases, the isotopic effect correlates with the nuclear magnetic spin. Here, we show nuclear spin effects using stable oxygen isotopes (^{16}O, ^{17}O, and ^{18}O) in two separate setups: an artificial dioxygen production system and biological aquaporin channels in cells. We observe that oxygen dynamics in chiral environments (in particular its transport) depend on nuclear spin, suggesting future applications for controlled isotope separation to be used, for instance, in NMR. To demonstrate the mechanism behind our findings, we formulate theoretical models based on a nuclear-spin-enhanced switch between electronic spin states. Accounting for the role of nuclear spin in biology can provide insights into the role of quantum effects in living systems and help inspire the development of future biotechnology solutions.

nuclear spin | isotope | spin–statistics | aquaporin | electrolysis

The role of spin in biological processes is a subject of great interest and scientific debate (1, 2). While the role of electron spin in photosynthesis (3–5), magnetoreception (6–9), the chiral-induced spin selectivity (CISS) effect in biology (10–12), and beyond (13–16) has been investigated, the role of the nuclear spin in biological processes is still unclear. With that said, large mass-independent fractionation (MIF) signatures in ions such as Mg^{2+} (17) and Hg^{2+} (18, 19) have been observed in biological environments. Many MIFs are related to nuclear spin. Chemically induced dynamic nuclear polarization (CIDNP) (20, 21) and the magnetic isotope effect (MIE) (22, 23) are two related effects linking the nuclear magnetic spin in a chemical reaction to the spin selectivity of the chemical process. Both phenomena express the dependence of the reaction rates on the nuclear spin and nuclear magnetic moment of the reactants. In former works (20, 24), in-depth theoretical analysis has produced a comprehensive model that accounts for this rate difference originating from specific processes at the atomic level. MIEs have been proposed as the mechanism behind MIF in living cells (17). Expression of an MIE can, for example, lead to MIF of isotopes, resulting from the spin conversion induced by hyperfine coupling (25), spin–orbit coupling (19, 26), and/or dipole–dipole interaction (27). In the current work, we expand the known chemical and biochemical effects of nuclear spin and propose a link between nuclear spin conversion of quantum states and biological processes which have distinct chirality.

Many vital biological molecules are chiral and appear in nature only as one of the two enantiomeric forms—living organisms are almost perfectly homochiral (28, 29). It is known that the electron spin and chirality are related through the CISS effect; depending on the handedness of the molecule, electrons of a certain spin can more easily traverse the molecule in one direction than in the other (1, 30). As an electron propagates through a chiral molecule or material, it moves in the overall direction of the net electric field but along a helical trajectory. This helical motion leads to an effective magnetic field, which acts on the magnetic moment of the electron by effective spin–orbit coupling, stabilizing one spin and destabilizing the other (1). The CISS effect was demonstrated with respect to electron spin but has not yet been studied in respect to nuclear spin. The effect, however, may extend beyond electron transport processes, via transport of protons, ions, and molecules through biological membranes in chiral channels. These chiral channels can generate effective fields: an electric field due to electrostatic effects, resulting from the amino acid charges and polarity (dictating the intrapore water orientation) (31) and\or a magnetic field from spin–orbit coupling [CISS effect (32)]. These fields could interact with the nuclear spin directly or indirectly [for instance, through the Stark effect (33)].

Nuclear spin transport (the directional movement of molecules with nonzero nuclear spin) is hard to manipulate and measure, as it averages out in a solution. Furthermore, it

Significance

This research provides a significant contribution to understanding the role of nuclear spin in biological processes. The experimental data and theoretical models presented demonstrate that nuclear spin can influence oxygen dynamics, suggesting the possibility of using nuclear spin to manipulate and control isotopic fractionation. These findings can lead to unique applications in biotechnology and open research avenues into the role of quantum effects in biology.

Author affiliations: [a]Department of Applied Physics, Hebrew University of Jerusalem, Jerusalem 91904, Israel; [b]Department of Plant & Environmental Sciences, The Alexander Silberman Institute of Life Sciences, Hebrew University of Jerusalem, Jerusalem 91904, Israel; [c]Institute of Science and Technology Austria, Klosterneuburg 3400, Austria; [d]The Lautenberg center for Immunology and Cancer Research, The Institute for Medical Research Israel-Canada, The Hebrew University Medical School, Jerusalem 91121, Israel; [e]Department of Earth and Planetary Sciences, Weizmann Institute of Science, Rehovot 76100, Israel; and [f]The Fredy & Nadin Herrman Institute of Earth Sciences, Hebrew University of Jerusalem, Jerusalem 91904, Israel

typically occurs over very short time scales and is extremely sensitive to the environment. However, there are a variety of chemical elements, which have both nonmagnetic and magnetic stable isotopes (NMI and MI, respectively). Using such isotopic systems, it is nonetheless possible to probe the nuclear spin effect in chemical processes (23–25). Our approach takes advantage of the different spin states and masses of naturally occurring oxygen isotopes: the NMI ^{16}O and ^{18}O that have zero nuclear spin and the MI ^{17}O that has a 5/2 nuclear spin. Oxygen was chosen also because of its significance in biological systems, where nuclear spin may play an important role. Using oxygen isotopes, two complementary experiments were performed, one in a controlled chemical environment and the other in a biological system of living cells. Both experiments provide evidence of a role for nuclear spin.

In both experiments, an aqueous solution that contains the three stable isotopes of oxygen was used. Comparing the behavior of these three isotopes allows us to observe nuclear spin interactions indirectly by measuring the isotopic ratios. The fact that the magnetic isotope ^{17}O is neither the lightest nor the heaviest isotope allows distinction between mass-dependent fractionation (MDF) and MIF resulting from the nuclear spin. We developed theoretical models, which reproduce the measured effects and provide mechanistic understanding. These models are based on rate equations where the MIs behave differently from the NMIs, namely in the accelerated ability to change electronic spin states due to hyperfine interactions between the nuclear and electron spins (24, 27, 34). Taken together, the experimental results and theoretical models open a path of exploration into the interaction of nuclear spin in chemical and biological environments.

Results

In expirement number one the effect of chirality was probed on the isotopic fractionation observed during water splitting. Previous works showed that the CISS effect enables the creation of a spin-selective electron current. This is achieved by coating the electrodes with a layer of homochiral molecules (32–37). Therefore, water electrolysis can be used as a simple probe into the interaction of nuclear spin with chiral molecules and electron spin. The electrolysis of water is the decomposition of water into dioxygen (O_2) and dihydrogen (H_2) gases due to the passage of electric current, described by the equation $2H_2O(l) \rightarrow 2H_2(g) + O_2(g)$. The O_2 gas is produced on the anode side, in the following oxidation reaction: $2OH^- \rightarrow \frac{1}{2}O_2 + H_2O + 2e^-$. Recent experiments show that O_2 production in the process is increased by creating a spin-selective current using chiral coatings as described above (38–41). In those experiments, CISS can enhance water-splitting efficiency using the electronic spin. In the current experiment, the behavior of nuclear spins involved in the process is studied.

The aqueous solution used in the process contains the three stable isotopes of oxygen (in natural abundance) which have known probabilities of participation in the electrolysis reaction, based on mass differences. Comparing the behavior of these three isotopes in the electrolysis reaction allows us to elucidate the role of the spin without the need to directly measure nuclear spin. Instead, isotopic ratios are quantified by mass spectrometry. The fractionation of O_2 gas produced in "conventional" electrolysis is known at a very high accuracy (42) to be of the type $1 + \delta^{17}O = \left(1 + \delta^{18}O\right)^{\lambda}$, where $\lambda = 0.5281 \pm 0.0015$ is the "mass exponent". The δ-notation is given by Eq. **1**, in which ^{1x}O is a rare isotope of oxygen (^{17}O, ^{18}O). It is usually expressed in ‰.

$$\delta^{1x}O = \left(\frac{\left(\frac{^{1x}O}{^{16}O}\right)_{sample}}{\left(\frac{^{1x}O}{^{16}O}\right)_{standard}} - 1 \right) \cdot 1000. \qquad [\mathbf{1}]$$

The postulate was that with an anode coated in chiral molecules, the mass exponent would deviate from the expected mass-dependent value of 0.5281. Such a deviation could either arise directly from the nuclear spin interacting with the chiral molecules or from the electron spin (passing through the chiral molecule) interacting with the oxygen nuclear spin. In both cases, deviation from the mass-dependent exponent would provide strong evidence for the importance of nuclear spin in the reactions involving chiral molecules. The isotope effect and its mass dependence are process dependent. Therefore, for comparison, the experiment was repeated using the same setup with a bare electrode (no molecular coating). The resulting mass exponents were $\lambda_{chiral} = 0.506 \pm 0.0014$ and $\lambda_{bare} = 0.510 \pm 0.0024$, which indeed are both different from the value quoted in Meijer and Li (42). Nonetheless, the chiral-coated electrode value is further from 0.5281 than that of the bare electrode, and the difference between the two is larger than 1σ. As presented in Fig. 1C, the $\frac{\delta^{17}O}{\delta^{18}O}$ ratio is lower in the O_2 produced when using a chiral-coated electrode: 0.5086 ± 0.00124 vs. 0.5127 ± 0.00248 for the bare electrode (calculated by sample average). When calculating using a linear fit to the values of $\delta^{17}O$ and $\delta^{18}O$ in each experiment (Fig. 1 A and B), the slope values are 0.5083 ± 0.00127 for the chiral-coated electrode vs. 0.5128 ± 0.00249 for the bare electrode (Fig. 1C). Under both methods of calculation, the difference is statistically significant (difference of more than 1σ, and P-values of $\ll 0.001$). Raw data are available in *SI Appendix*. The samples were measured by isotope ratio mass spectrometry (IRMS).

A complimentary experiment with a chiral-coated electrode was also performed, in which the electrolyte used was either natural water (99.76% ^{16}O) or enriched natural water (9% ^{17}O or 9% ^{18}O), and mean current was measured throughout the process. According to mass-dependent kinetic effects, we would expect to see a linear relation between the average current and the mass of the enriched isotope; instead, we see that the ^{17}O samples had the lowest current, followed by ^{18}O and then ^{16}O (*SI Appendix*, Fig. S1 and Table S2).

The second experiment was done with living human cells, thus exploring the effect in functioning biological organisms. Within the cell's membrane, there are designated channels for water transfer called aquaporins (AQPs). As well as the AQPs, there is also limited diffusion of water directly through the cell membrane. The AQPs are highly restrictive and transfer only water molecules, excluding ions and other solutes (43). The AQP channel contains left handed alpha – helixes which generates a highly chiral shape (44). The water molecule (which contains the oxygen isotopes) closely interacts with the channel when passing through it (43, 45).

We studied the uptake of the different water isotopologues $H_2{}^{16}O$, $H_2{}^{17}O$ and $H_2{}^{18}O$ by living cells. In this way, we could examine the interaction of nuclear spin with the chiral aquaporin channel. Cells with natural aquaporin channels (AQP-4) within their membrane were incubated in an isotonic medium highly enriched with ^{17}O and ^{18}O at 37 °C (*SI Appendix*, Table S3). The incubation lasted 20 min, a time that was deemed long enough to allow the isotopes to enter the cells but short enough so as not to reach equilibrium with the extracellular medium. Throughout the experiment, isotonic conditions were carefully maintained to ensure a gradual entrance of water into the cells. After incubation, the intracellular water was extracted
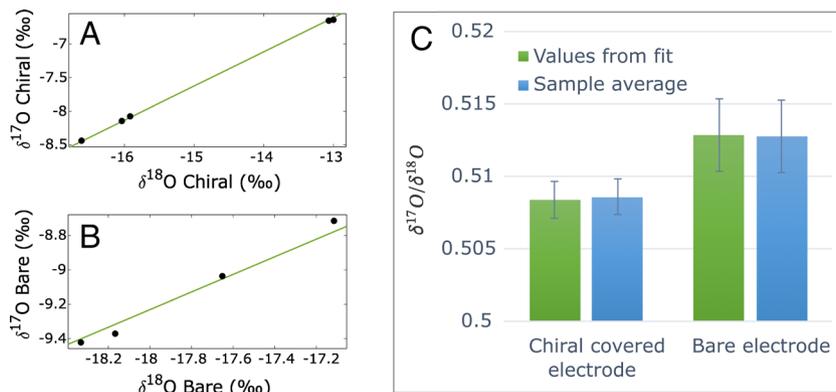
Fig. 1. Electrolysis results. (*A* and *B*) Linear fit for chiral-covered and bare electrode values, respectively. Goodness of fit: *A*-R^2 = 0.999, *B*-R^2 = 0.976. (*C*) $\frac{\delta^{17}O}{\delta^{18}O}$ values in the evolved oxygen from fit values (green), or calculated as sample average (blue), with SD shown in error bars. Data from nine experiments in total. Values for the chiral covered electrode are 0.5083±0.00127 (fit) and 0.5086±0.00124 (average). For the bare electrode, values are 0.5128±0.00249 (fit) and 0.5127±0.00248 (average). *P*-values are ≪0.001.

using cold aqua trapping (CAT). A calibration measurement of the isotopes was done using IRMS (46).

Fig. 2*A* schematically shows the procedure of water uptake by the cells followed by cell lysis and extraction of the intracellular water, which was measured using a cavity ring-down spectroscope (CRDS). The isotopic composition of the intracellular fluid (C) was compared to that of the extracellular medium (M) (Fig. 2*B*). Two media were used, both highly enriched in $H_2^{17}O$ and $H_2^{18}O$ but with a different $^{17}O/^{18}O$ ratio. In one medium (source 1), the initial proportion of $H_2^{17}O$ was slightly higher than $H_2^{18}O$, whereas in the other medium (source 2), the proportion of $H_2^{18}O$ was slightly higher than $H_2^{17}O$ (raw data in the *SI Appendix*). Fig. 2*B* shows a clear bias in source 1 toward the uptake of $H_2^{17}O$, which carries the magnetic isotope. The comparison between the cell and medium isotope concentrations ratio is statistically significant, resulting in a *P* value of less than 0.001. For source 2, no definite bias is observed; there could be multiple explanations for this to occur. First, it is possible that the cells incubated in source 2 were more reactive and reached equilibrium with the medium at a faster rate, leading to a smaller visible effect. Second, it is possible that the initial concentrations of the isotopes in the medium led to this result. The second possibility is explored further in the theoretical model.

Theoretical Models. The results presented above indicate different probabilities or rates for processes involving magnetic and nonmagnetic oxygen isotopes. The nuclear spin of the magnetic isotope can prompt spin conversion in the water's hydrogens (27, 47, 48) from ortho (triplet) quantum state to para (singlet) and vice versa. This interconversion can be explained by the radical pair model (34), where nuclear magnetic moments can induce singlet-triplet mixing in radical pairs. Moreover, the ortho–para states have different effective dipole moments (33), which influence their response to an electric field, suggesting different rates for moving through the AQP channel. These ideas can be translated into rate equations to describe both the chemical process of electrolysis and the biological process of water passage through AQP.

Electrolysis. It has previously been shown that the efficiency of O_2 production in electrolysis is increased in a chiral environment (38–41). The mechanism suggested to explain this increase involves the suppression of H_2O_2 creation, which is a by-product of a competing reaction involving OH* radicals. Simply put, two OH* radicals can combine to create either O_2 or H_2O_2, depending on whether their spins are parallel or antiparallel (Fig. 3). Conforming with allowed spin transitions, a pair of OH* radicals with parallel
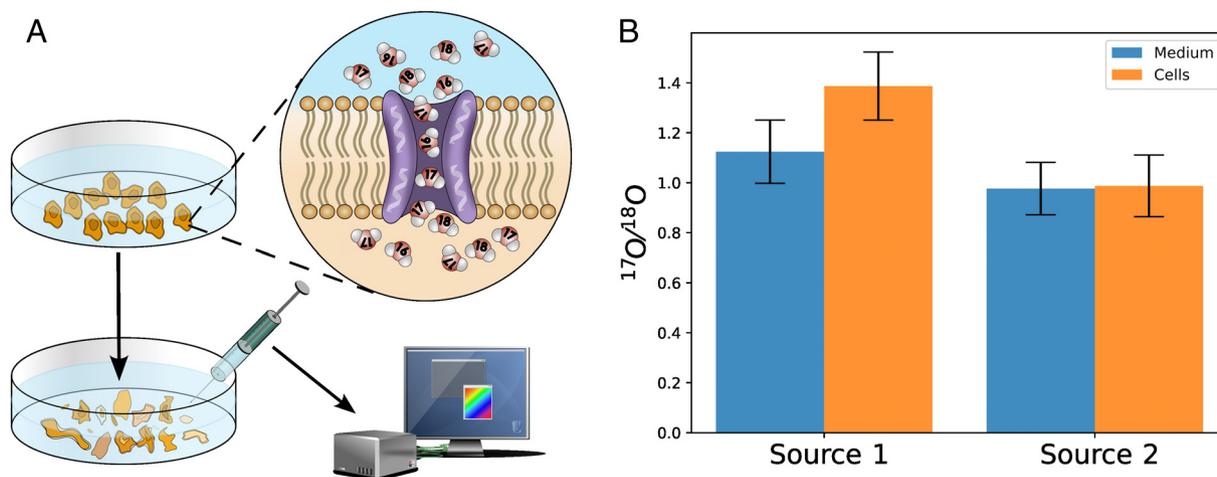
Fig. 2. AQP experiment- method and results. (*A*) Schematic of the water entrance process into the cells and the extraction of the intracellular water from the exploded cells used for the measurements. (*B*) The isotopic concentration ratios between ^{17}O and ^{18}O of the intracellular water referred to as cells and the extracellular water referred to as medium, for each of the two sources.
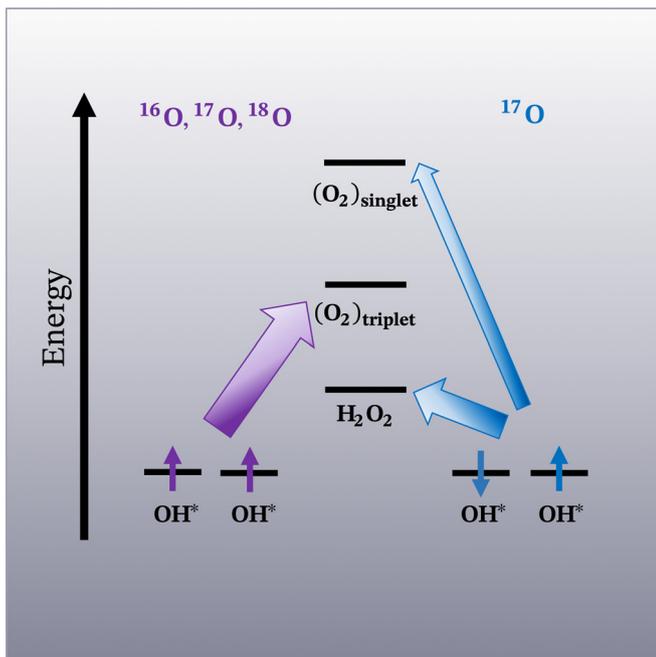
Fig. 3. Parallel spin pairs can create only triplet O_2, while antiparallel pairs can create either H_2O_2 or singlet O_2. Moreover, creation of H_2O_2 is thermodynamically favored over creation of singlet O_2.
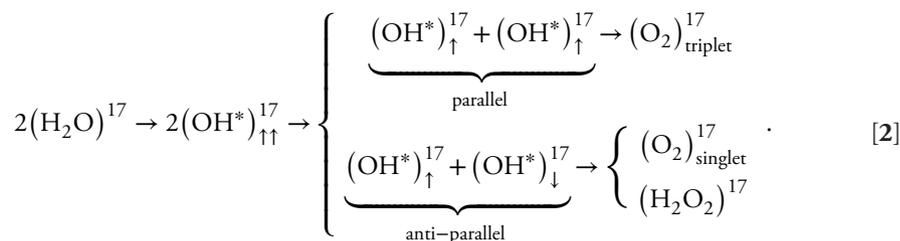
spin pairs can create triplet O_2, which is the ground state for molecular O_2, while an antiparallel pair can create either H_2O_2 or singlet $O_2{}^*$. The pairs can also backreact to create H_2O (*SI Appendix*) (49–51).

OH* radicals are created on the surface of the anode by the donation of an electron from an OH^- ion. For a bare electrode, electrons with up or down spin would enter at similar rates. However, when the anode is coated with a monolayer of homochiral molecules, the spins of these radicals will preferentially be parallel to each other, due to the CISS effect (10, 11, 13, 24–26). Furthermore, when reactions occur on surfaces, the stability of germinate radical pairs is enhanced (52, 53), which works in conjunction with the CISS effect to elongate the lifetime of OH radical pairs on the surface of the chiral electrode. In this manner, the reaction can occur before diffusion randomizes the effect. Radical pairs with parallel spins will create only triplet O_2, unless there is a mechanism whereby an up spin can convert to a down spin.

In our proposed model, the ^{17}O isotope enables just such a mechanism due to the hyperfine interaction between its nuclear spin and the radical hole spin. The rate of conversion from up to down spin will be accelerated in radicals containing a magnetic

*Although it is correct that an anti-parallel pair can also create triplet O2 (if the spins are added instead of subtracted), our paper adopts the reasoning of Mtangi et al. (38), as shown in our reproduction of the figure in their paper (Fig. 3). In any case, since the enthalpy of formation of H2O2 is significantly lower than both triplet and singlet O2, the final product will predominantly consist of H2O2. Therefore, the conclusion in this paper remains essentially unchanged: Eq. 3 would simply need a small correction to η, which would be negligible since we would still have η ≪ 1.

oxygen isotope (^{17}O) compared to NMIs (^{16}O and ^{18}O). As a result, the MI creates more H_2O_2 than NMIs, at the expense of creating O_2. When measuring the final O_2 product, the MI will be depleted relative to the NMIs (Eq. **2**), in agreement with the results of the electrolysis experiment. In CIDNP experiments, the mechanism by which this can occur has been studied extensively by N. J. Turro and others, showing that radical pairs with nuclear spin states that promote intersystem crossing between singlet and triplet states are more likely to form singlet radical pairs and their by-products (in our case, this corresponds to parallel or antiparallel spin pairs) (52–55). Although it is of course true that spin relaxation can also convert parallel-spin radical pairs into antiparallel pairs, the chiral environment has been shown to significantly elongate spin relaxation times (nano to microseconds) (56). As discussed in previous works, the timescales are extended since they are determined by the kinetics of adsorption and desorption, and the effect is similar to that of magnetized surfaces (57–60). As a result, the interconversion of radical pairs mediated by the ^{17}O nuclear spin can occur at faster rates than spin relaxation. Since H_2O_2 has a lower vapor pressure than H_2O, the purification procedure prior to the IRMS measurement, which removes water vapor, should also remove H_2O_2. Therefore, we do not expect H_2O_2 to affect the analysis of O_2 isotopologues.

$$2(H_2O)^{18} \to 2(OH^*)^{18}_{\uparrow\uparrow} \to (O_2)^{18}_{triplet}$$

$$2(H_2O)^{17} \to 2(OH^*)^{17}_{\uparrow\uparrow} \to \begin{cases} \underbrace{(OH^*)^{17}_{\uparrow} + (OH^*)^{17}_{\uparrow} \to (O_2)^{17}_{triplet}}_{parallel} \\ \underbrace{(OH^*)^{17}_{\uparrow} + (OH^*)^{17}_{\downarrow}}_{anti-parallel} \to \begin{cases} (O_2)^{17}_{singlet} \\ (H_2O_2)^{17} \end{cases} \end{cases} \quad [2]$$

We formulate a series of rate equations to encapsulate the dynamics of this result, of which we present only the final product (detailed derivations are given in *SI Appendix*). When the rate equations are solved at a steady state, the ratio of the final MI to NMI O_2 products, normalized by their concentration in the original water, is indeed smaller than unity (Eq. **3**).

$$\frac{\left(\frac{(O_2)^{17}}{(H_2O)^{17}}\right)}{\left(\frac{(O_2)^{18}}{(H_2O)^{18}}\right)} = \frac{\left(\frac{(O_2)^{17}}{(H_2O)^{17}}\right)}{\left(\frac{(O_2)^{16}}{(H_2O)^{16}}\right)}$$

$$= \frac{2+\eta}{3}\left(\frac{\tilde{k}^{17} + \frac{\beta}{2}}{2\tilde{k}^{17} + \frac{\beta}{2}}\right) + \eta\left(\frac{\tilde{k}^{17}}{2\tilde{k}^{17} + \frac{\beta}{2}}\right) < 1. \quad [3]$$

The parameter η accounts for the difference in rates of singlet O_2 creation relative to H_2O_2, where $\eta \ll 1$. $\tilde{k}^{17}$ denotes the rate of conversion between up and down spins for the OH* radicals, and β is the probability of two OH* combining to form a product. Overall, this model can explain the deviation from the expected value of λ when using a chiral-coated electrode.

Water passage through AQP. We developed rate equations for the uptake of water molecules through AQP into the cells. The water passage rate through the AQP [~1 ns (43)] is considered
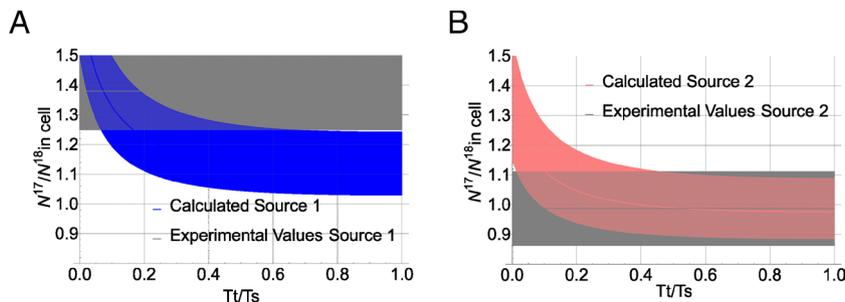
Fig. 4. The ratio between the number of MI and the NMI molecules which entered the cell via the AQP channel as a function of the relative difference between the time it takes a singlet or a triplet to move through the channel. Source 1 (*A*) and source 2 (*B*) represent the calculated ratios given initial concentrations according to the two different mediums in the experimental part. Shaded areas correspond to error bars; the curves present the central values. As we can see, the calculated values overlap with the experimental results and approach the initial concentration ratios when reaching identity between triplet and singlet transfer rates.

to be much faster than the proton exchange rate [~1 ms (61)]. Therefore, we will treat ortho- and para-water states as separate entities (62). As water molecules pass the AQP they exhibit strong local polarization effects and are sequentially reoriented (63). It is suggested that breakage of hydrogen bonds is also involved in the water flow (43). Molecules with a larger dipole moment will be easier to rotate, and it will be easier to break their hydrogen bonds. The ortho (triplet) state's dipole moment can be twice as large as the singlet (para). For simplicity, we assume that all triplet states have identical dipole moments. Therefore, we presume that the triplet-state water will be transferred faster through the AQP than the singlet state ($T_t < T_s$ where $T_{s/t}$ is the time for a singlet/triplet water molecule to go through the AQP). We assume a steady state in the near-AQP region, which is different from the whole bath because an AQP extracts a very small number of molecules from the bath at a given time.

$$\frac{dN_s^{17}}{dt} = -\frac{\rho_s^{17}}{T_s} + A + k_{t\to s}^{17} N_t^{17} - k_{s\to t}^{17} N_s^{17}. \qquad [4]$$

$$\frac{dN_t^{17}}{dt} = -\frac{\rho_t^{17}}{T_t} + 3A + k_{s\to t}^{17} N_s^{17} - k_{t\to s}^{17} N_t^{17}. \qquad [5]$$

Eqs. **4** and **5** are the rate equations for triplet and singlet states of the ^{17}O water isotopes (similarly for ^{16}O, ^{18}O). N_s^{17} is the number of singlet water molecules with ^{17}O in the near-AQP region (similarly to triplet), ρ_s^{17} is the relative number of N_s^{17} in the H_2O^{17} near AQP population, A is the rate for a singlet molecule to enter the near AQP region (due to the equilibrium ratios of singlets and triplets, A is multiplied by 3 in the triplet case (Eq. **5**), and $k_{t\to s}$ is the time constant for triplet-to-singlet conversion and vice versa.

Therefore, the population that will enter the cell can be calculated as the following:

$$N_{s,in}^{17} = \frac{\rho_s^{17}}{T_s} \cdot t; \; N_{t,in}^{17} = \frac{\rho_t^{17}}{T_t} \cdot t. \qquad [6]$$

The experimentally measured R values can be expressed as:

$$R_{in}^{17} = \frac{n(O^{17})}{n(O^{16})} = \frac{N_{s,in}^{17} + N_{t,in}^{17}}{N_{s,in}^{16} + N_{t,in}^{16}}. \qquad [7]$$

The model allows calculation of the ratio $\frac{R_{in}^{17}}{R_{in}^{18}}$ as a function of the relative difference between the passage time of triplet and singlet

water through the AQP (detailed calculations in the *SI Appendix*). Note that these ratios are of the same order as the dipole moment ratios for water in different spin states. This gives credibility to our discussion; a more detailed theoretical investigation along the lines suggested below is left to future studies. The results of the rate equations are presented in Fig. 4. We can see that for $\frac{T_t}{T_s}$ which varies between $\sim 0.1 - 0.6$ and, our calculations fall within the experimental results. The developed model is nonlinear and depends on the initial ratios of the isotopes in the bath. This means the effect can be enhanced by enrichment of the bath with more ^{17}O. The relative time difference range we calculated here can correspond to the energy shift that ortho and para water experience in a DC electric field (Stark effect) (33). The chiral AQP channel generates an effective electric field which acts on the dipole of the water molecules. These models could explain our experimental results and provide a starting point for avenues of nuclear spin research in biology.

Discussion

The electrolysis experiment results yield a deviation from the expected mass exponent λ. Moreover, they indicate that when using an anode covered in chiral molecules, the $\frac{\delta^{17}O}{\delta^{18}O}$ ratio in the evolved O_2 is smaller. This implies discrimination against ^{17}O in the chiral environment. The difference in mass between the isotopes is not expected to result in different fractionation with and without chiral molecules. If anything, we would expect a preference for the production of O_2 containing the lighter oxygen isotope when the electrode is coated with an additional barrier of molecules, chiral or not (due to faster diffusion of isotopically light species). Hence, this selectiveness seems to be a result of the different nuclear spin. The associated theoretical model provides a relatively simple explanation for this phenomenon, revealing that the decrease in O_2 product containing the MI ^{17}O is associated with the nuclear spin undergoing hyperfine interaction, while favoring the MI in the other reaction products. An interesting prediction of this hypothesis is that the MIF should be even greater in an alkaline medium, in which the OH^--mediated reaction is promoted. The results of the complementary electrolysis experiment (with initial isotopic enrichment of the electrolyte) suggest that the magnetic nuclear spin of ^{17}O increases the overpotential needed to complete the reaction (all experiments were performed under constant applied voltage, so a decrease in current implies an increase in overpotential). We hypothesize that this is due to the increase in production of H_2O_2, which produces a higher overpotential due to the spin-forbidden reaction.

Turro experiments in micelles (52, 53), showing the importance of surface-mediated reactions, imply that biological systems provide an ideal environment for observing nuclear spin–related phenomena, which is a fascinating direction for further research. Recently, the efficiency of the hydrolysis reaction has been improved using a magnetized catalyst to enhance the O-H cleavage (64), suggesting a future experiment where a chiral-coated electrode is also magnetized to probe the synergistic effect of the two modifications. An experimental setup has already been created in our lab to facilitate such an investigation.

The AQP results seem puzzling at first glance. However, when taking the initial concentrations into account, the theoretical model predictions explain the observed differences. To further test the model, experiments with an even larger initial enrichment of $H_2^{17}O$ relative to $H_2^{18}O$ will be performed in future work. In that case, one would expect to see an even larger bias of $\frac{R^{17}}{R^{18}}$ in the cells compared to the medium. Delving deeper, the raw data show that in source 1, the proportions of both $H_2^{17}O$ and $H_2^{18}O$ are smaller in the cells than in the medium, while in source 2, the opposite is true. It is highly unlikely that the MDF differs between experiments, and a plausible explanation, therefore, is that in source 1 the uptake of the enriched extracellular water was slower than in source 2. If this is true, we can deduce that in general there is a preference for the uptake of heavier isotopes. But this would mean that if only mass-dependent effects were important, we would expect the ratio $\frac{R^{17}}{R^{18}}$ to be smaller in the cells than in the medium, which is clearly not the case in source 1. So, we are left with the conclusion that there exists a mechanism that is not mass dependent that creates a preference for the faster transport of $H_2^{17}O$ relative to $H_2^{18}O$. Within short enough time scales (before equilibrium), we can see the effect of this mechanism in the deviation of the ratio $\frac{R^{17}}{R^{18}}$ between the medium and the cells.

The experimental data shows an MIF related to the nuclear spin of oxygen isotopes in both systems. We present theoretical models which can describe the interplay between nuclear spin and these results. Although the precise details of the two models differ, both are based on the assumption that the magnetic nuclear spin of ^{17}O enables accelerated intersystem crossing between electronic spin states, leading to a difference in reaction or transfer rates. The reasoning behind choosing nuclear spin as the focus of the explanations is that both experiments involved a chiral environment, which is closely related to spin through the CISS effect. Further experiments are undoubtedly required to clarify this hypothesis.

The phenomenon of NMR is widely used in research, industry, and medicine (65–70). This process relies on the use of MIs, since NMIs do not interact with the magnetic field and therefore cannot produce a signal. Aside from ^1H, the MIs used in NMR are extremely rare and hard to purify (71). Here, we show a possible method for the enrichment of ^{17}O, which could have significant importance to noninvasively determine the metabolic rate of oxygen in living organisms (72, 73). Beyond known applications, further exploration of nuclear spin in biology can have exciting implications for the future.

Materials and Methods

Electrolysis. The experimental setup was built similarly to the one described by Bhattacharya et al. (74) and is shown in *SI Appendix*, Fig. S2. We designed a U-shaped electrolysis cell, in which H_2 escapes to the atmosphere from the left leg, and O_2 is collected into the vacuum system in the right leg. The electrodes are Platinum foils, with and without adsorbed L-alpha helix polyalanine (L-AHPA) molecules. In all electrolysis experiments, regular deionized tap water is used. Helium is used as a carrier gas. Oxygen isotope composition is later measured (by IRMS) in the collected gas and compared to the composition measured in the absence of the chiral molecules. Prior to IRMS measurement the O_2 was purified by trapping water and pumping away helium. The electrolyte used is H_2SO_4 or $Na_2SO_4(+HCl)$, with the same proton concentration. A Nafion membrane is positioned between the two legs to prevent the migration of H_2 gas and SO_2 produced at the cathode to the anode side, where they could contaminate the O_2 sample. In the ion source of the IRMS, even small amounts of H_2 may form a molecular ion HO_2^+ with mass 33, thus overlapping with the $^{16}O^{17}O^+$ molecular ion.

Water Passage through AQP.

CAT-IRMS/IRLS-based analysis of isotope water flux and fractionation in live cells. For the analysis of the influx rate of ^{17}O-water and ^{18}O-water into cells under isotonic conditions, we prepared two types of mixed isotope media. The first medium contained 0.44836 g ^{17}O-water, 0.21152 g ^{18}O-water, and 6.81 mg Roswell Park Memorial Institute (RPMI) powder. The second medium was prepared using 0.468116 g ^{17}O-water, 0.1912 g ^{18}O-water, and 6.8 mg RPMI powder. Cell plates with a similar number of MCF7 cells ($\pm10\%$) were incubated at 37 °C for 20 min with each of the media to allow the isotopically labeled water from the media to enter the cells (46). After the incubation, the labeled water media was removed, and the cells were washed three times with PBS. The cells were then mixed with double distilled water and frozen before being thawed and collected for measurements. Cell samples, standards, and references were then diluted and sent for oxygen ratio measurement by IRMS.

Isotopic measurements of $^{18}O/^{16}O$ and $^{17}O/^{16}O$ of intracellular water (diluted by up to 200,000 times) were performed on a Picarro L2140-i CRDS and scaled and calibrated against the international standards VSMOW2 ($\delta^{17}O = 0.00‰$, $\delta^{18}O = 0.00‰$) and SLAP2 ($\delta^{17}O = -29.74‰$, $\delta^{18}O = -55.55‰$; ref. 75). The precision (1σ) for the international standards, which were measured on every eighth analysis (i.e., after seven unknown individual samples), was 0.14‰ and 0.29‰ for $\delta^{17}O$ and $\delta^{18}O$ of VSMOW2, respectively, and 0.28‰ and 0.42‰ for $\delta^{17}O$ and $\delta^{18}O$ of SLAP2, respectively. Samples were injected ten times in high precision mode (9 min per injection) using a clean 10 µL SGE autosampler syringe with a fixed needle, and signal levels ranged between 19,000 and 21,000 ppmv.

Data, Materials, and Software Availability. All study data and materials are included in the article and/or *SI Appendix*.

1. R. Naaman, Y. Paltiel, D. H. Waldeck, Chiral molecules and the electron spin. *Nat. Rev. Chem.* **3**, 250–260 (2019), 10.1038/s41570-019-0087-1.
2. Y. Kim *et al.*, Quantum biology: An update and perspective. *Quantum Rep.* **3**, 80–126 (2021), 10.3390/QUANTUM3010006.
3. R. E. Blankenship, *Molecular mechanisms of photosynthesis* (John Wiley, Sons Inc, Tempe, AZ, USA, ed. 2, 2014).
4. F. Perrin, Théorie quantique des transferts d'activation entre molécules de même espèce. Cas des solutions fluorescentes. *Annales de Physique* **10**, 283–314 (1932), 10.1051/ANPHYS/193210170283.
5. G. Panitchayangkoon *et al.*, Direct evidence of quantum transport in photosynthetic light-harvesting complexes. *Proc. Natl. Acad. Sci. U.S.A.* **108**, 20908–20912 (2011), 10.1073/pnas.1105234108.
6. A. Schulten, Swenberg Klaus, E. Charles, Weller, A biomagnetic sensory mechanism based on magnetic field modulated coherent electron spin motion. *Zeitschrift für Physikalische Chemie* **111**, 1–5 (1978).
7. P. J. Hore, H. Mouritsen, The radical-pair mechanism of magnetoreception. *Annu. Rev. Biophys.* **45**, 299–344 (2016), 10.1146/annurev-biophys-032116-094545.
8. I. Carmeli, K. S. Kumar, O. Heifler, C. Carmeli, R. Naaman, Spin selectivity in electron transfer in photosystem I. *Angewandte Chemie* **126**, 9099–9104 (2014), 10.1002/ange.201404382.

9. E. M. Gauger, E. Rieper, J. J. L. Morton, S. C. Benjamin, V. Vedral, Sustained quantum coherence and entanglement in the avian compass. *Phys. Rev. Lett.* **106**, 1–4 (2011), 10.1103/PhysRevLett.106.040503.

10. K. Michaeli, N. Kantor-Uriel, R. Naaman, D. H. Waldeck, The electron's spin and molecular chirality-how are they related and how do they affect life processes? *Chem. Soc. Rev.* **45**, 6478–6487 (2016), 10.1039/c6cs00369a.

11. H. M. Levy *et al.*, The effect of spin exchange interaction on protein structural stability. *Phys. Chem. Chem. Phys.* **24**, 29176–29185 (2022), 10.1039/d2cp03331c.

12. Z. Xie *et al.*, Spin specific electron conduction through DNA oligomers. *Nano Lett.* **11**, 4652–4655 (2011), 10.1021/nl2021637.

13. M. A. Van Der Horst, K. J. Hellingwerf, Photoreceptor proteins, "star actors of modern times": A review of the functional dynamics in the structure of representative members of six different photoreceptor families. *Acc. Chem. Res.* **37**, 13–20 (2003), 10.1021/AR020219D.

14. R. A. G. Cinelli *et al.*, Coherent dynamics of photoexcited green fluorescent proteins. *Phys. Rev. Lett.* **86**, 3439 (2001), 10.1103/PhysRevLett.86.3439.

15. S. Shi, P. Kumar, K. F. Lee, Generation of photonic entanglement in green fluorescent proteins. *Nat. Commun.* **8**, 1–7 (2017), 10.1038/s41467-017-02027-9.

16. H. B. Gray, J. R. Winkler, Electron tunneling through proteins. *Quarterly Rev. Biophys.* **36**, 341–372 (2003), 10.1017/S0033583503003913.

17. V. K. Koltover *et al.*, Magnetic-isotope effect of magnesium in the living cell. *Doklady Biochem. Biophys.* **442**, 12–14 (2012), 10.1134/S1607672912010048.

18. J. D. Blum, L. S. Sherman, M. W. Johnson, Mercury isotopes in earth and environmental sciences. *Annu. Rev. Earth Planet. Sci.* **42**, 249–269 (2014), 10.1146/annurev-earth-050212-124107.

19. L. C. Motta, A. D. Chien, A. E. Rask, P. M. Zimmerman, Mercury magnetic isotope effect: A plausible photochemical mechanism. *J. Phys. Chem. A* **124**, 3711–3719 (2020), 10.1021/acs.jpca.0c00661.

20. H. R. Ward, Chemically induced dynamic nuclear polarization (CIDNP). I. The phenomenon, examples, and applications. *Acc. Chem. Res.* **5**, 18–24 (1972), 10.1021/ar50049a003.

21. H. Fischer, Chemically induced dynamic nuclear polarization. *Zeitschrift für Naturforschung A* **25**, 1957–1963 (1970), 10.1002/9780470034590.emrstm0077.pub2.

22. N. J. Turro, W. R. Cherry, Magnetic isotope and magnetic field effects on chemical reactions. Sunlight and soap for the efficient separation of carbon-13 and carbon-12 isotopes. *Am. Chem. Soc.* **43**, 7432–7434 (1978), https://pubs.acs.org/doi/pdf/10.1021/ja00491a061.

23. A. L. Buchachenko, Magnetic isotope effect: Nuclear spin control of chemical reactions. *J. Phys. Chem. A* **105** (2001), 10.1021/jp011261d.

24. G. J. Kavarnos, N. J. Turro, Photosensitization by reversible electron transfer: Theories, experimental evidence, and examples. *Chem. Rev.* **86**, 401–449 (1986).

25. A. Buchachenko, *Magnetic Isotope Effect in Chemistry and Biochemistry* (Nova Science Publishers Inc., New York, 2009).

26. I. V. Khudyakov, Y. A. Serebrennikov, N. J. Turro, Spin-orbit coupling in free-radical reactions: On the way to heavy elements. *Chem. Rev.* **93**, 537–570 (1993).

27. B. Meier *et al.*, Spin-isomer conversion of water at room temperature and quantum-rotor-induced nuclear polarization in the water-endofullerene H$_2$O@C$_{60}$. *Phys. Rev. Lett.* **120**, 1–6 (2018), 10.1103/PhysRevLett.120.266001.

28. D. G. Blackmond, The origin of biological homochirality. *Cold Spring Harb. Perspect. Biol.* **2**, a002147 (2010), 10.1101/CSHPERSPECT.A002147.

29. S. Toxvaerd, Origin of homochirality in biosystems. *Int. J. Mol. Sci.* **10**, 1290–1299 (2009), 10.3390/IJMS10031290.

30. R. Naaman, D. H. Waldeck, Chiral-induced spin selectivity effect. *J. Phys. Chem. Lett.* **3**, 16, 2178–2187, 10.1021/jz300793y (2012).

31. M. Bernardi *et al.*, Human aquaporin 4 gating dynamics under axially oriented electric-field impulses: A non-equilibrium molecular-dynamics study. *J. Chem. Phys.* **149**, 245102 (2018), 10.1063/1.5044665.

32. R. Naaman, D. H. Waldeck, Spintronics and chirality: Spin selectivity in electron transport through chiral molecules. *Annu. Rev. Phys. Chem.* **66**, 263–281 (2015), 10.1146/annurev-physchem-040214-121554.

33. D. A. Horke, Y. P. Chang, K. Długołęcki, J. Küpper, Separating para and ortho water. *Angewandte Chemie* **53**, 11965–11968 (2014), 10.1002/anie.201405996.

34. H. R. Ward, Chemically induced dynamic nuclear polarization (CIDNP). I. The phenomenon, examples, and applications. *Acc. Chem. Res.* **5**, 18–24 (1972).

35. K. Ray, S. P. Ananthavel, D. H. Waldeck, R. Naaman, Asymmetric scattering of polarized electrons by organized organic films of chiral molecules. *Science* **283**, 814–816 (1999), 10.1126/science.283.5403.814.

36. B. Göhler *et al.*, Spin selectivity in electron transmission through self-assembled monolayers of double-stranded DNA. *Science* **331**, 894–897 (2011), 10.1126/science.1199339.

37. J. J. Wei *et al.*, Molecular chirality and charge transfer through self-assembled scaffold monolayers. *J. Phys. Chem. B* **110**, 1301–1308 (2006), 10.1021/jp055145c.

38. W. Mtangi, V. Kiran, C. Fontanesi, R. Naaman, Role of the electron spin polarization in water splitting. *J. Phys. Chem. Lett.* **6**, 4916–4922 (2015), 10.1021/acs.jpclett.5b02419.

39. W. Mtangi *et al.*, Control of electrons' spin eliminates hydrogen peroxide formation during water splitting. *J. Am. Chem. Soc.* **139**, 2794–2798 (2017), 10.1021/jacs.6b12971.

40. W. Zhang, K. Banerjee-Ghosh, F. Tassinari, R. Naaman, Enhanced electrochemical water splitting with chiral molecule-coated Fe3O4 nanoparticles. *ACS Energy Lett.* **3**, 2308–2313 (2018), 10.1021/acsenergylett.8b01454.

41. K. B. Ghosh *et al.*, Controlling chemical selectivity in electrocatalysis with chiral CuO-coated electrodes. *J. Phys. Chem. C* **123**, 3024–3031 (2019), 10.1021/acs.jpcc.8b12027.

42. H. A. J. Meijer, W. J. Li, The use of electrolysis for accurate δ17O and δ18O isotope measurements in water. *Isot. Environ. Health Stud.* **34**, 349–369 (1998), 10.1080/10256019808234072.

43. K. Murata *et al.*, Structural determinants of water permeation through aquaporin-1. *Nature* **407**, 599–605 (2000), 10.1038/35036519.

44. S. Törnroth-Horsefield *et al.*, Structural mechanism of plant aquaporin gating. *Nature* **439**, 688–694 (2006), 10.1038/nature04316.

45. B. L. De Groot, T. Frigato, V. Helms, H. Grubmüller, The mechanism of proton exclusion in the aquaporin-1 water channel. *J. Mol. Biol.* **333**, 279–293 (2003), 10.1016/J.JMB.2003.08.003.

46. A. Saragovi *et al.*, Analysis of cellular water content in T cells reveals a switch from slow metabolic water gain to rapid water influx prior to cell division. *J. Biol. Chem.* **298**, 101795 (2022), 10.1016/j.jbc.2022.101795.

47. S. Meiboom, Nuclear magnetic resonance study of the proton transfer in water. *J. Chem. Phys.* **34**, 375–388 (1961), 10.1063/1.1700960.

48. H. N. Yeung, A. H. Lent, Proton transverse relaxation rate of 17O-enriched water. *Magn. Reson. Med.* **5**, 87–92 (1987), 10.1002/mrm.1910050112.

49. X. Zhang *et al.*, Disproportionation channel of the self-reaction of hydroxyl radical, OH + OH → H2O + O revisited. *J. Phys. Chem. A* **124**, 3993–4005 (2020), 10.1021/acs.jpca.0c00624.

50. G. Altinay, R. G. Macdonald, Determination of the rate constant for the OH(X2Π) + OH(X2Π) → H2O + O(3P) reaction over the temperature range 295 to 701 K. *J. Phys. Chem. A* **118**, 38–54 (2014), 10.1021/jp409344q.

51. M. Sangwan, E. N. Chesnokov, L. N. Krasnoperov, Reaction CH 3 + OH studied over the 294–714 K temperature and 1–100 bar pressure ranges. *J. Phys. Chem. A* **116**, 8661–8670 (2012), 10.1021/jp305070c.

52. N. J. Turro *et al.*, Additive effects on the CIDNP, cage effect, and exit rate of micellized radical pairs. *J. Phys. Chem.* **91**, 4544–4548 (1987), 10.1021/j100301a024.

53. J. C. Scaiano, E. B. Abuin, L. C. Stewart, Photochemistry of benzophenone in micelles. Formation and decay of radical pairs. *J. Am. Chem. Soc.* **104**, 5673–5679 (1982), 10.1021/ja00385a020.

54. K. C. Hwang, H. D. Roth, N. J. Turro, K. M. Welsh, Enhancement or suppression of CIDNP intensities by a second magnetic nucleus: Interplay between g factor difference, external magnetic field, and hyperfine coupling constants. *J. Phys. Organic Chem.* **5**, 209–217 (1992), 10.1002/poc.610050406.

55. K. C. Hwang, N. J. Turro, C. Doubleday, Investigation of the kinetic window for generation of 13C T0-S CIDNP derived from long-chain biradicals by tuning the rates of bimolecular scavenging and intersystem crossing. *J. Am. Chem. Soc.* **113**, 2850–2853 (1991), 10.1021/ja00008a008.

56. K. Santra, Q. Zhang, F. Tassinari, R. Naaman, Electric-field-enhanced adsorption of chiral molecules on ferromagnetic substrates. *J. Phys. Chem. B* **123**, 9443–9448 (2019), 10.1021/acs.jpcb.9b07987.

57. A. Ziv *et al.*, AFM-based spin-exchange microscopy using chiral molecules. *Adv. Mater.* **31**, e1904206 (2019), 10.1002/adma.201904206.

58. Y. Kapon *et al.*, Evidence for new enantiospecific interaction force in chiral biomolecules. *Chem* **7**, 2787–2799 (2021), 10.1016/j.chempr.2021.08.002.

59. Y. Paltiel, G. Cuniberti, Role of exchange interactions in the magnetic response and intermolecular recognition of chiral molecules. *Nano Lett.* **20**, 7077–7086 (2020), 10.1021/acs.nanolett.0c02216.

60. H. T. Fridman, J. Dehnel, S. Yochelis, E. Lifshitz, Y. Paltiel, Spin-exciton delocalization enhancement in multilayer chiral linker/quantum dot structures. *J. Phys. Chem. Lett.* **10**, 3858–3862 (2019), 10.1021/acs.jpclett.9b01433.

61. D. Mammoli *et al.*, Challenges in preparing, preserving and detecting para-water in bulk: Overcoming proton exchange and other hurdles. *Phys. Chem. Chem. Phys.* **17**, 26819–26827 (2015), 10.1039/c5cp03350k.

62. V. I. Tikhonov, A. A. Volkov, Separation of water into its ortho and para isomers. *Science* **296**, 2363 (2002), 10.1126/science.1069513.

63. M. Jensen, U. Röthlisberger, C. Rovira, Hydroxide and proton migration in aquaporins. *Biophys. J.* **89**, 1744–1759 (2005), 10.1529/biophysj.104.058206.

64. Q. Huang *et al.*, Spin-enhanced OH Cleavage in electrochemical water oxidation.pdf. *Angewandte Chemie* **62**, e202300469 (2023), 10.1002/anie.202300469.

65. M. Pellecchia, D. S. Sem, K. Wüthrich, NMR in drug discovery. *Nat. Rev. Drug Dis.* **1**, 211–219 (2002), 10.1038/nrd748.

66. P. A. Bottomley, NMR imaging techniques and applications: A review. *Rev. Sci. Instruments* **53**, 1319 (1998), 10.1063/1.1137180.

67. E. Hatzakis, Nuclear magnetic resonance (nmr) spectroscopy in food science: A comprehensive review. *Comp. Rev. Food Sci. Food Safety* **18**, 189–220 (2019), 10.1111/1541-4337.12408.

68. D. Marion, An introduction to biological NMR spectroscopy. *Mol. Cell. Proteomics* **12**, 3006–3025 (2013), 10.1074/mcp.O113.030239.

69. P. A. Bottomley, Human in vivo NMR spectroscopy in diagnostic medicine: clinical tool or research probe? *Radiology* **170**, 1–15 (1989), 10.1148/RADIOLOGY.170.1.2642336.

70. A. G. Palmer, NMR characterization of the dynamics of biomacromolecules. *Chem. Rev.* **104**, 3623–3640 (2004), 10.1021/CR030413T/ASSET/CR030413T.FP.PNG_V03.

71. R. Verardi, N. J. Traaseth, L. R. Masterson, V. V. Vostrikov, G. Veglia, Isotope labeling for solution and solid-state NMR spectroscopy of membrane proteins. *Adv. Exp. Med. Biol.* **992**, 35–62 (2012), 10.1007/978-94-007-4954-2_3.

72. C. Losert, M. Peller, P. Schneider, M. Reiser, Oxygen-enhanced MRI of the brain. *Magn. Reson. Med.* **48**, 271–277 (2002), 10.1002/mrm.10215.

73. X. H. Zhu, W. Chen, In vivo oxygen-17 NMR for imaging brain oxygen metabolism at high field. *Prog. Nucl. Magn. Reson. Spectrosc.* **59**, 319–335 (2011), 10.1016/J.PNMRS.2011.04.002.

74. S. K. Bhattacharya, J. Savarino, B. Luz, Mass-dependent isotopic fractionation in ozone produced by electrolysis. *Analytical Chem.* **81**, 5226–5232 (2009), 10.1021/ac900283q.

75. J. A. G. Wostbrock, E. J. Cano, Z. D. Sharp, An internally consistent triple oxygen isotope calibration of standards for silicates, carbonates and air relative to VSMOW2 and SLAP2. *Chemical Geol.* **533**, 119432 (2020), 10.1016/j.chemgeo.2019.119432.